NASA TECHNICAL NOTE

NASA TN D-6286

LOW-FREQUENCY PLASMA NOISE FROM THE ELECTRON-BOMBARDMENT ION THRUSTER

by Allan J. Cohen

Lewis Research Center
Cleveland, Ohio 44135

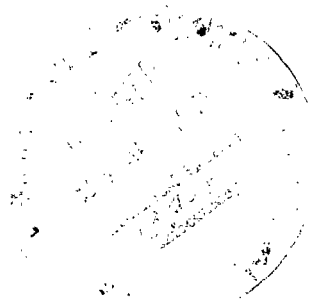

NATIONAL AERONAUTICS AND SPACE ADMINISTRATION • WASHINGTON, D. C. • APRIL 1971

1. Report No.	2. Government Accession No.	3. Recipient's Catalog No.
NASA TN D-6286		

4. Title and Subtitle	5. Report Date
LOW-FREQUENCY PLASMA NOISE FROM THE ELECTRON-BOMBARDMENT ION THRUSTER	April 1971
	6. Performing Organization Code

7. Author(s)	8. Performing Organization Report No.
Allan J. Cohen	E-6053
	10. Work Unit No.
	120-26

9. Performing Organization Name and Address	11. Contract or Grant No.
Lewis Research Center National Aeronautics and Space Administration Cleveland, Ohio 44135	
	13. Type of Report and Period Covered
12. Sponsoring Agency Name and Address	Technical Note
National Aeronautics and Space Administration Washington, D. C. 20546	14. Sponsoring Agency Code

15. Supplementary Notes

16. Abstract

Low-frequency plasma noise from a mercury electron bombardment ion thruster was studied for several magnetic-field configurations. Frequency spectra of the plasma noise were recorded from the operating thruster and a correlation study comparing probe separation with signal time delay was made. A critical magnetic field was determined from ion chamber performance and relative plasma noise measurements. Rotation of the plasma noise was found from the correlation study with a direction of rotation determined by the magnetic-field direction. Correlation of the plasma noise along field lines was also observed with no time delay. A cusp magnetic field in only a portion of the discharge chamber was found to suppress plasma noise but no improvement of thruster performance was observed.

17. Key Words (Suggested by Author(s))	18. Distribution Statement
Electron propulsion Electron bombardment ion thruster Plasma Plasma noise	Unclassified - unlimited

19. Security Classif. (of this report)	20. Security Classif. (of this page)	21. No. of Pages	22. Price*
Unclassified	Unclassified	26	$3.00

*For sale by the National Technical Information Service, Springfield, Virginia 22151

LOW-FREQUENCY PLASMA NOISE FROM THE ELECTRON-BOMBARDMENT ION THRUSTER

by Allan J. Cohen

Lewis Research Center

SUMMARY

Low-frequency plasma noise from a mercury electron-bombardment ion thruster was studied for several magnetic field configurations. Frequency spectra of the plasma noise were recorded from the operating thruster and a correlation study comparing probe separation with signal time delay was made. A critical magnetic field was determined from ion chamber performance and relative plasma noise measurements. Rotation of the plasma noise was found from the correlation study with a direction of rotation determined by the magnetic field direction. Correlation of the plasma noise along field lines was also observed with no time delay. A cusp magnetic field in only a portion of the discharge chamber was found to suppress plasma noise but no improvement of thruster performance was observed.

INTRODUCTION

In the ion thruster (refs. 1 to 3) the bombardment of neutral atoms by electrons produces an ionized gas in a cylindrical discharge chamber. An axial magnetic field is used to obtain a high discharge efficiency. A plasma formed in such a chamber will diffuse radially outward, crossing the magnetic field lines. As a result of the $J \times B$ body force, the plasma will tend to rotate under the influence of the magnetic field. The bombardment thruster exhibits low-frequency plasma noise (ref. 4). Similar noise has been observed in many plasma physics experiments (see review article, ref. 5). These disturbances or fluctuations are linked to the drifting magnetized plasma and have been termed drift waves. They are discussed in detail in this report.

A large increase in the plasma noise level above a particular value of magnetic field strength was reported in reference 6. Also, the ion number density leveled off. The increase of plasma noise at this critical magnetic field strength was also throught to be

related to the observed leveling off of the discharge energy per beam ion (ref. 7). Kaufman (ref. 8) suggested that increased (or anomalous) diffusion greater than the classical level would occur above the critical magnetic-field strength. In reference 4 a cusp magnetic field in the discharge chamber was found to suppress noise beyond the critical field strength.

In the present investigation a mercury electron-bombardment ion thruster was tested with three different magnetic field shapes (1) a uniform magnetic field, (2) a divergent magnetic field, and (3) a divergent magnetic field with a superimposed cusp magnetic field. The third field configuration was used to study noise suppression by means of plasma stabilization. The purpose of this study was to determine if the plasma discharge properties are affected by the noise and over what range of magnetic field strength noise is important.

APPARATUS AND PROCEDURE

Thruster

Thruster configurations. - Figure 1 shows the three thruster configurations tested. The basic thruster was a cylindrical discharge chamber with a perforated pair of grids on the downstream end. The 10-centimeter-long discharge chamber contained a 20-centimeter-diameter anode and a cathode filament. In thruster configurations (1) and (2), the mercury vapor entered through a centerline hole and was distributed by a baffle. In configuration (2), a second anode was placed in the back on the centerline as in reference 9. This 8-centimeter-diameter rear anode had a 4-centimeter-diameter hole in the center. In configuration (3), the mercury vapor entered the chamber through numerous holes in the back plate.

The first configuration (fig. 1(a)) has two identical magnet coils placed on the front of and behind the thruster. These coils produced a fairly uniform magnetic field (±10 percent) throughout most of the discharge chamber. The second configuration (fig. 1(b)) has a single magnet coil behind the thruster. An iron filing map of this divergent magnetic field is presented in figure 2. In the third configuration, a magnetic quadrupole was used in the rear portion of the discharge chamber in addition to the single coil. This combination produced the magnet-field configuration shown in the iron filing map presented in figure 3. In this thrid configuration the chamber had a smaller main anode placed nearer the grids and the cusp field was confined by the iron pole pieces to the rear of the discharge plasma. Thus the anode was located in a region dominated by the divergent field alone. The magnetic field strengths for the divergent configurations (2 and 3) were measured at the cathode location.

Electrical configuration. - An electrical schematic for the thruster is shown in figure 4. The high voltage and accelerator supplies were operated at 2000 and 1000 volts, respectively, for thruster performance data but were not used during plasma noise measurements. A constant discharge voltage of 50 volts was used throughout the tests. An electrically heated porous tungsten plug vaporizer was used to introduce mercury propellant into the thruster. The cusp field supply was operated in the third configuration only. The thruster was operated either on the main anode or rear anode (for thruster (2)) using the switch shown in figure 4.

Facility

The thruster was operated in a metal bell jar that was 1 meter in diameter, with the beam directed into a vacuum tank that was $1\frac{1}{2}$ meters in diameter 5 meters long. The vacuum tank, described in detail in reference 10, was operated at a pressure of about 7×10^{-6} torr.

Langmuir Probes

Four Langmuir probes were used in the tests. A typical probe is shown in figure 5(a). The exposed sensing tip had a length of about 0.4 centimeter and a diameter of 2.54×10^{-3} centimeter. The position of the four probes is shown in figure 5(b). The probes penetrated the discharge chamber walls as shown and were set radially halfway between the wall and the chamber axis. Two probes, A and C, were shifted by 120° on the circumference from the other two, B and D. Also, probe set A and C and set B and D were separated longitudinally 5 centimeters.

Measurements

In the tests the thruster performance was determined in terms of discharge energy per beam ion as a function of magnetic-field strength and propellant utilization efficiency. The discharge energy per beam ion (eV/ion) is equal to the discharge power divided by the beam current. The propellant utilization efficiency is equal to the beam current divided by the equivalent mercury flow rate into the thruster.

Figure 6 shows electrical schematics for the two methods used in the noise investigation. In figure 6(a) the noise signal, sensed by a Langmuir probe, was applied to a filter. The filter removed the low-frequency (120 Hz) thruster power supply ripple from

the plasma noise. The remaining signal was observed with either a spectrum analyzer or rms voltmeter. The spectrum analyzer displays plasma noise strength as a function of frequency. The rms voltmeter was used to determine the total noise level sensed by the Langmuir probe.

In figure 6(b) the electrical schematic for the correlation experiment is shown. Two tuned circuits picked out a single identical frequency component from each of two probe noise signals and compared them on a dual beam oscilloscope. The sweeps of the upper beam fall on top of each other giving a sine wave on oscilloscope photographs traces. If the other probe signal is delayed in a nonrandom manner then the lower beam also will be a clean sine wave with a given phase shift. For azimuthally separated probes, the phase shift determines the frequency of rotation of the plasma noise. Further details are given in the next section and in reference 11. In a few instances measurements were taken by a current probe (transformer), which was placed around the anode lead to pick up AC (plasma noise) signals.

RESULTS AND DISCUSSION

Uniform Field Operation

Discharge energy per beam ion is plotted in figure 7 as a function of magnetic field strength for the thruster with a uniform field configuration. The discharge losses drop rapidly with increasing field strength and level off at 2.7 milliteslas at a discharge energy per beam ion of 310 electron volts. The neutral flow rate was 240 milliamperes equivalent flow (assuming singly ionized mercury), and the beam current was 140 milliamperes. Discharge energy per beam ion as a function of propellant utilization is shown in figure 8. At 85 percent propellant utilization efficiency, the discharge energy per beam ion was about 400 electron volts. This performance is not as good as that reported for present thrusters (ref. 12), as a consequence of a uniform magnetic field.

Figure 9 shows photographs of oscilliscope traces of the frequency spectra of the plasma noise detected from Langmuir probe B from the uniform field thruster. The thruster was operated at a constant discharge current of 1 ampere. No change in the noise data (same spectra shape as well as relative magnitude) was found when the high voltage and accelerator voltage were switched off (no ion beam), so all noise data were taken without high voltages applied. This test was accomplished using a transformed pickup on the main anode lead. Spectra were recorded for different magnetic-field strengths and compared for conditions with the beam both on and off. In figure 9(a) a 120-hertz peak, due to the thruster power supply, is visible on the photograph. A zero peak, which is always placed on traces from the spectrum analyzer, and the mirror

image of the 120-hertz peak are also visible. The gain of the spectrum analyzer is not high enough for this trace to display the plasma noise from the thruster. Thus, the 120-hertz peak is very strong relative to the plasma noise from the thruster. The photograph in figure 9(b) was taken with a filter set to suppress signals below 150 hertz. When the gain of the spectrum analyzer was increased, the plasma noise became visible.

In figure 10 typical frequency spectra from the uniform-field thruster are shown for two different magnetic-field strengths. The thruster was again operated at a discharge current of 1 ampere and again probe B was the noise sensor. The vertical gain is adjusted to obtain the full spectrum on the photographs. No concentration of signal noise energy at a single frequency (as in fig. 9(a)) was found in this part of the tests. The broad spectrum of noise found was concentrated around zero frequency as shown by these photographic data.

The amplitude of the plasma noise was next measured with an rms voltmeter. A filter was set to suppress all noise below 150 hertz. The magnetic field strength was varied above and below 2.7 millitesla (the suspected critical magnetic field strength). The discharge current was adjusted to give a constant beam current of 140 milliamperes. This kept the plasma density constant throughout the measurements. Figure 11 is a plot of relative noise level in volts as a function of magnetic-field strength. A rise in the noise level occurred above 2.7 millitesla. This is the same field strength at which the discharge energy per beam ion leveled off (see fig. 7), thus indicating a relationship between the plasma noise increase and the performance (determined by plasma discharge conditions) of the ion thruster. Thus, for this configuration, the value of 2.7 millitesla can be regarded as the critical magnetic field.

In figure 12 photographs from a dual beam oscilloscope are presented. The vertical settings varied between 1 and 200 millivolts per centimeter. The horizontal setting (representing time) was set at about 50 microseconds per centimeter. Noise signals were taken with probes A and B except where noted. These signals passed through identically tuned circuits. The dual beam oscilloscope triggered on the upper beam so that all the individual traces of this beam fall on top of each other giving a sine wave at the frequency of the tuned circuit. If the lower signal is also a sine wave, then correlation (consistent phase separation) of the two signals has occurred. The figures are labeled according to the magnetic field (2.7 mT is the critical value), the signal frequency, and the phase shift (either leading or lagging the upper trace). The data are also labeled N or R referring to whether the magnetic field was normal or reversed.

Figure 12(a) shows a correlation for a magnetic field strength of 3.9 millitesla with a phase lead of 125°. Figure 12(b) shows a 125° phase lag corresponding to operation with a reversed magnetic field. Both correlation are for a signal frequency of 4.7 kilohertz. The only difference in the data is that the magnetic field was reversed for these two photographs, which caused a reversal in phase shift. Because the probes were 120°

apart, it is concluded that the disturbance is rotating in the thruster under the influence of the magnetic field at a rotational frequency of about 4.7 kilohertz. In figures 12(c) and (d) the same magnetic field strength was used and correlation of the 6- and 3-kilohertz components of the noise signal was investigated. Phase shifts of 150° and 84° were found. With the inferred rotational frequency of 4.7 kilohertz, calculated phase shifts of 153° and 77° were expected at these test frequencies. The results are in good agreement, which checks the inferred rotational frequency.

For figure 12(e) the neutral flow rate was increased from the 150-milliampere rate used throughout the correlation study to over 500 milliamperes. The result was a lack of correlation (no clear sine wave in the lower trace) presumably because of neutral damping of the signal in an arc length less than 120°.

In figures 12(f) and (g) the signal is compared at probes B and D. These probes were spaced along the field lines (see fig. 5). There is correlation but no phase shift between the detected noise components. Hence, the disturbance traveled along the field line without measurable time delay.

In figures 12(h) and (i) correlation occurs at a magnetic-field strength of 2.1 millitesla (below the critical field). Based on the 120° spatial phase positions, the disturbance was rotating at 3.6 kilohertz. This is a lower rotational frequency than found for the magnetic-field strength of 3.9 millitesla. In figure 12(j) a magnetic field strength of 1.8 millitesla was used and a phase shift of 207° found. This shift corresponds to rotation at a still lower frequency of 2.7 kilohertz. At a magnetic field strength of 1.5 millitesla (fig. 12(k)), the rotation appears to have disappeared, presumably because the magnetic field strength is too weak. Figure 12(l) shows lack of measurable phase shift along field lines from probes B and D at a magnetic field strength of 1.8 millitesla.

Nonuniform Field Operation

In figure 13 discharge energy per beam ion is plotted as a function of magnetic field strength for the thruster with the divergent magnetic field. The curve has a minimum at 2.8 millitesla (magnetic-field strength was measured at the cathode). The discharge energy per beam ion was 225 electron volts at this field strength. The neutral flow rate was 280 milliamperes, and the beam current was 200 milliamperes, giving a propellant utilization of 71 percent. The corresponding curve of discharge energy per beam ion as a function of propellant utilization is shown in figure 14. At 90-percent propellant utilization, the discharge energy per beam ion was 260 electron volts. This performance is comparable to present mercury bombardment ion thrusters (ref. 12).

Figure 15 is a typical frequency spectrum for nonuniform field operation. The noise pickup was by a current probe on the anode lead. No filter was used to suppress power

supply noise. A number of these photographs were taken for different magnetic field strengths at a constant discharge current. The spectra were similar to those found for uniform-field operation. A plot of relative noise level as a function of magnetic field strength was made based on the values that occurred at a frequency of 3 kilohertz. This plot is shown in figure 16. The rise of noise occurred beyond 2.4 millitesla very close to the minimum of the discharge energy per beam ion. It was concluded that the relation found before holds for nonuniform field operation as well as for uniform field operation: that is, that a leveling off of the discharge losses occurs at the same magnetic-field strength as a rise in plasma noise.

The thruster with a divergent magnetic-field configuration was next run on the rear anode (see fig. 1). The baffle that spread the mercury flow partially shielded the rear anode from a direct path to the cathode. The main anode was rendered ineffective by electrically connecting it to the thruster body which was at cathode potential. In figure 17 discharge energy per beam ion is presented as a function of magnetic-field strength for rear-anode operation. The curve levels off at about 2.4 millitesla, close to the value found with main anode operation. The neutral flow was 555 milliamperes and the beam current was 200 milliamperes, giving a propellant utilization of 36 percent. In figure 18 discharge energy per beam ion is plotted as a function of propellant utilization. At 70-percent utilization, the discharge energy per beam ion was 574. This, of course, is very poor performance for an ion thruster.

Frequency spectrum measurements of the low-frequency plasma signal for the thruster with divergent field and rear-anode operation are shown in figure 19. Because of poor synchronization between oscilloscope and spectrum analyzer, a sharp rise on the right side of the trace occurred that was unrelated to the noise measurement. A concentration of noise energy at about 2 kilohertz was found above the background plasma noise at an onset value of about 2.4 milliteslas. This is at nearly the same value of magnetic-field strength at which the discharge energy per beam ion leveled off, and it can therefore be defined as the critical field strength for this configuration.

After the preceding tests, a short correlation study of the plasma noise from the thruster with the divergent magnetic-field configuration and normal anode was undertaken. The data of figure 20 were taken from the dual beam oscilloscope with signals from probe set A and B and set B and D through the tuned circuits. The settings are 100 millivolts per centimeter on the vertical axis and 50 microsecond per centimeter on the horizontal axis. For the data presented in these figures the thruster was run on the main anode. There was no 2-kilohertz peak when run on the main anode. Figures 20(a) and (b) show a leading and lagging phase shift of about 120° for probes A and B, which were azimuthally displaced by 120°. This is due to a reversal of the magnetic field. The disturbance was evidently rotating at 4.7 kilohertz. Figure 20(c) shows a phase shift of 45° from probes B and D (separated longitudinally). The phase shift being other

than zero was probably due to the probes being set parallel to the centerline and the magnetic field being divergent. The phase shift would arise because the disturbance must cross field lines from probes B to D.

For the data presented in figure 21, the thruster was operated on the rear anode. The probe signal was filtered with a bandpass filter to remove noise at frequencies above and below the 2-kilohertz peak. In figure 21(a) the filtered signal from probes C and D was observed on the dual-beam oscilloscope. There was no phase shift even though these probes were separated 120° azimuthally. In figure 21(b) the 2-kilohertz signal was observed on the oscilloscope to be coming from probe C and a transformer on the main anode lead. A 90° phase shift was observed. Whether the 2-kilohertz signal represents a traveling or standing wave with phase shift in the radial direction could not be determined.

Cusp Field Operation

Next a cusp magnetic field was added to the thruster previously operated with a divergent magnetic field (see fig. 1). The cusp field was confined by the quadrupole electromagnet to the upstream portion of the thruster. The portion of the thruster near the grids was affected primarily by the divergent magnetic field. The total field in the forward portion of the thruster decreased in strength as the radial position increased.

A plasma noise study was made. Figure 22 shows the frequency spectrum of the plasma noise from the thruster operating with a nonuniform field and with and without the additional cusp magnetic field. Without the cusp field, the data of figures 22(a) and (b) was observed. The data represent typical plasma noise patterns previously found for the thruster. Probe A was used as the plasma noise sensor. A filter was used for the data of figure 22(b) but not for that of figure 22(a). When the cusp field was energized with a 10-ampere current, the plasma noise diminished to a low level as shown in both figures 22(c) and (d). The two cases presented are for axial fields greater than and less than the critical magnetic field of 2.7 milliteslas found previously. The cusp field strength halfway between adjacent poles was 0.55 millitesla per ampere. When an rms voltmeter was used, it was found that the noise diminished in strength for the two cases presented by a factor of 20 to 30 compared with operation with no cusp field.

It is noteworthy that suppression of noise occurred with the thruster operating at greater than and less than the critical magnetic field strength. Noise suppression also occurred in the cusp axial magnetic geometry in which the cusp field was confined to only a portion of the configuration. However, no improvement of thruster performance was observed with the addition of a noise suppressing cusp field.

SUMMARY OF RESULTS

Values of discharge energy per beam ion and relative low-frequency noise strength as a function of magnetic field strength were determined for an ion thruster. The noise level increased and the discharge energy per beam ion leveled off at about the same magnetic field strength. This critical value of magnetic field strength did not act as a separator of any other behavior observed in this investigation.

Frequency spectra of the plasma noise from the ion thruster with a cylindrical anode did not show any peaks but showed a concentration of broad-band noise around zero frequency. A peak at 2 kilohertz was found, however, in the plasma noise from the divergent field thruster operating on a back anode.

A correlation study indicated a rotation of the fluctuations in the uniform and non-uniform field thrusters operating with a cylindrical anode. This study also indicated no time delay to the fluctuations along magnetic-field lines. Furthermore, the 2-kilohertz peak found in this study showed a noise phase separation in the radial direction.

Use of a cusp field in a portion of the thruster resulted in noise suppression. This noise suppression was highly effective in reducing the noise strength in the experiment by a factor of 20 to 30. The cusp field worked as a noise suppressor even though it was contained in only a portion of the thruster geometry. No improvement in performance, however, was noted.

Lewis Research Center,
National Aeronautics and Space Administration,
Cleveland, Ohio, December 30, 1970,
120-26.

REFERENCES

1. Kaufman, Harold R.: An Ion Rocket With an Electron-Bombardment Ion Source. NASA TN D-585, 1961.

2. Reader, Paul D.: Investigation of a 10-Centimeter-Diameter Electron-Bombardment Ion Rocket. NASA TN D-1163, 1962.

3. Milder, Nelson L.: A Survey and Evaluation of Research on the Discharge Chamber Plasma of a Kaufman Thruster. Paper 69-494, AIAA, June 1969.

4. Cohen, Allan J.: An Electron Bombardment Thruster Operated With a Cusped Magnetic Field. NASA TN D-5448, 1969.

5. Chen, Francis F.: The Leakage Problem in Fusion Reactors. Sci. Am., vol. 217, no. 1, July 1967, pp. 76-88.

6. Domitz, Stanley: Experimental Evaluation of a Direct-Current Low-Pressure Plasma Source. NASA TN D-1659, 1963.

7. Cohen, Allan J.: Onset of Anomalous Diffusion in Electron-Bombardment Ion Thrustor. NASA TN D-3731, 1966.

8. Kaufman, Harold R.: Electron Diffusion in a Turbulent Plasma. NASA TN D-1324, 1962.

9. Knauer, W.; Poeschel, R. L.; King, H. J.; and Ward, J. W.: Discharge Chamber Studies For Mercury Bombardment Ion Thrusters. Hughes Research Labs. (NASA CR-72440), Sept. 1968.

10. Keller, Thomas A.: NASA Electric Rocket Test Facilities. 1960 Seventh National Symposium on Vacuum Technology Transactions. Pergamon Press, 1961, pp. 161-167.

11. Cohen, Allan J.: Anomalous Diffusion in a Plasma Formed From the Exhaust Beam of an Electron-Bombardment Ion Thruster. NASA TN D-4758, 1968.

12. Bechtel, Robert T.: Discharge Chamber Optimization of the Sert II Thruster. J. Spacecraft Rockets, vol. 5, no. 7, July 1968, pp. 795-800.

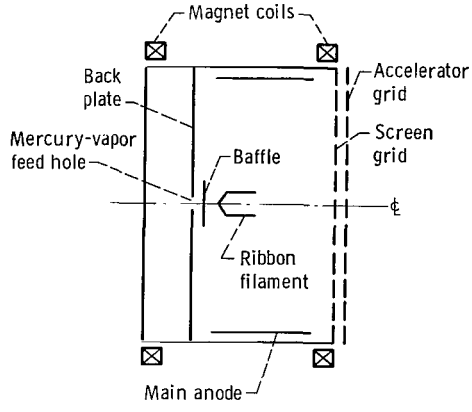

(a) Uniform field (configuration (1)).

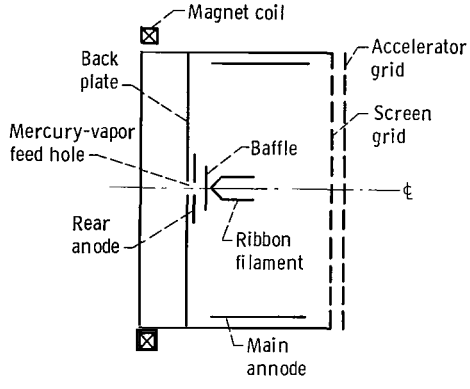

(b) Nonuniform field with rear anode (configuration (2)).

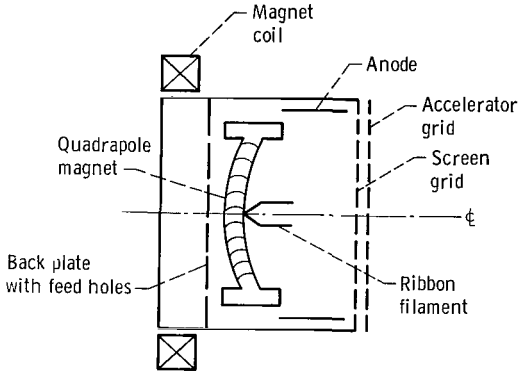

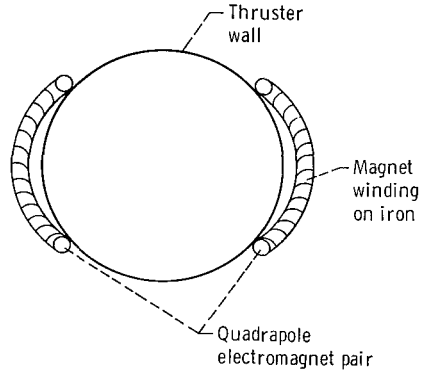

(c) Nonuniform field with quadrapole (cusp) pair added (configuration (3)).

Figure 1. - Three mercury bombardment thrustor configurations tested. Main anode diameter, 20 centimeters; chamber length, 10 centimeters.

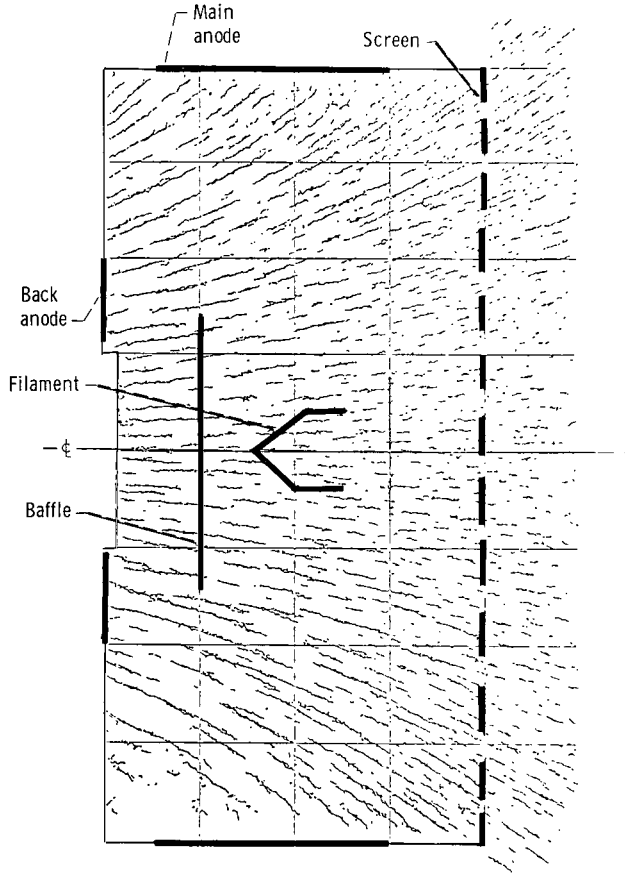

Figure 2. - Iron filing map of divergent magnetic field for thruster configuration (2) (fig. 1(b)) showing internal thruster components.

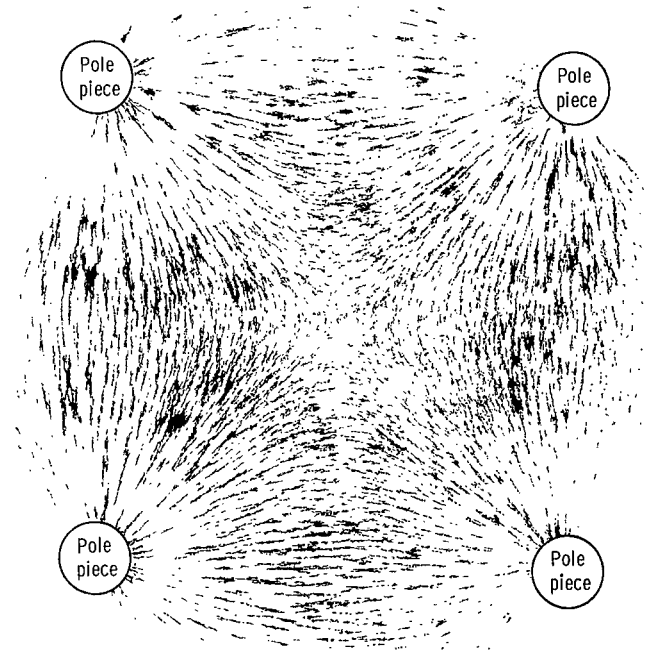

Figure 3. - Iron-filing map of cusped field of thruster configuration (3) showing pole pieces. Plane of figure is normal to thruster axis.

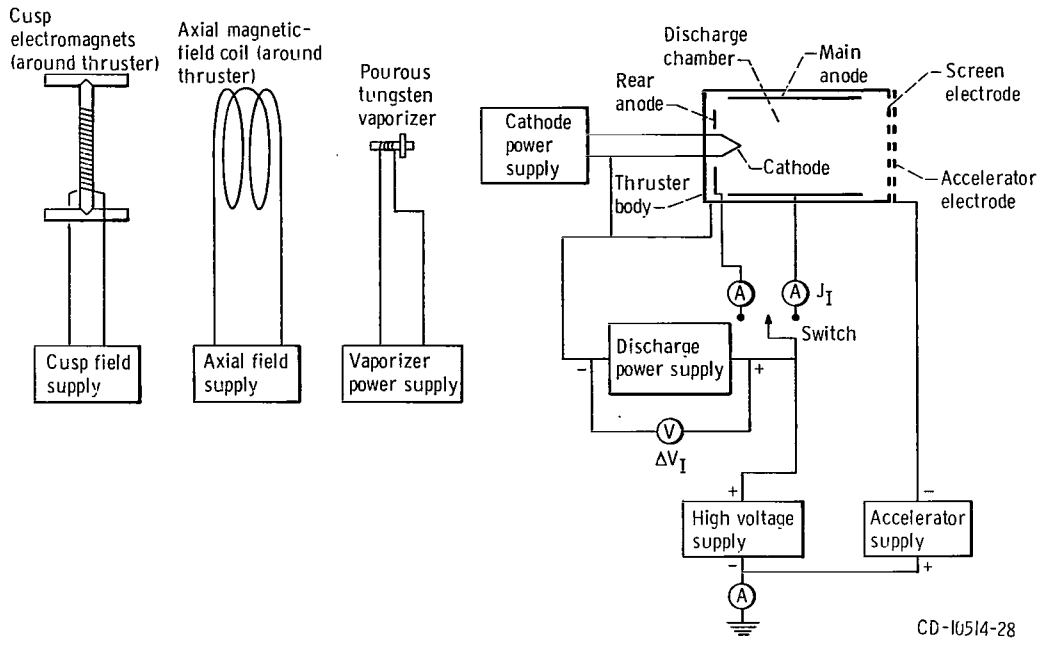

Figure 4. - Electrical schematic for thruster.

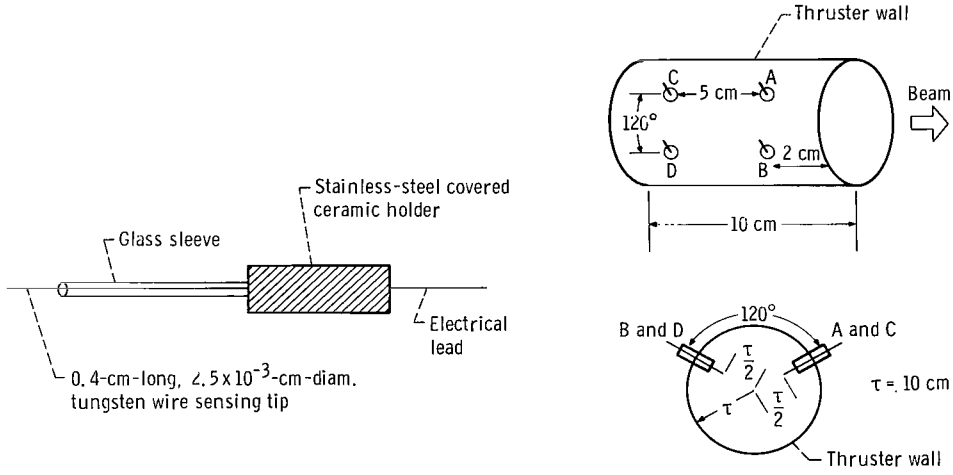

(a) Langmuir probe.

(b) Position of Langmuir probes.

Figure 5. - Langmuir probe details for noise investigation.

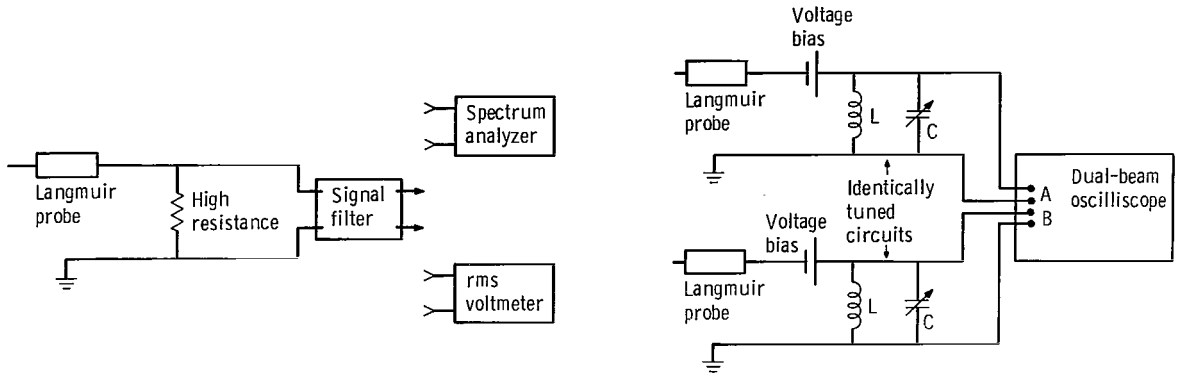

(a) Noise test circuit.

(b) Correlation test circuit using two Langmuir probes.

Figure 6. - Electrical schematics for noise investigation.

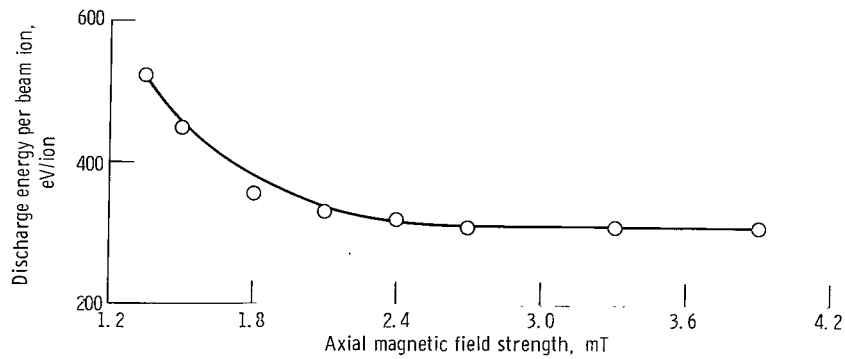

Figure 7. - Discharge energy per beam ion as function of magnetic field strength for uniform field operation. Beam current, 140 milliamperes; neutral flow, 240 milliamperes.

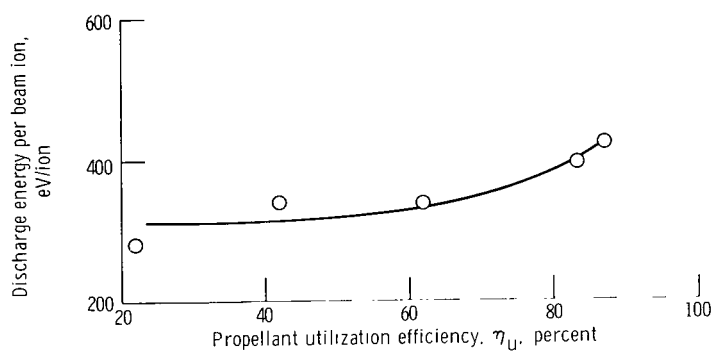

Figure 8. - Discharge energy per beam ion as function of propellant utilization efficiency for uniform-field operation. Neutral flow, 240 milliamperes.

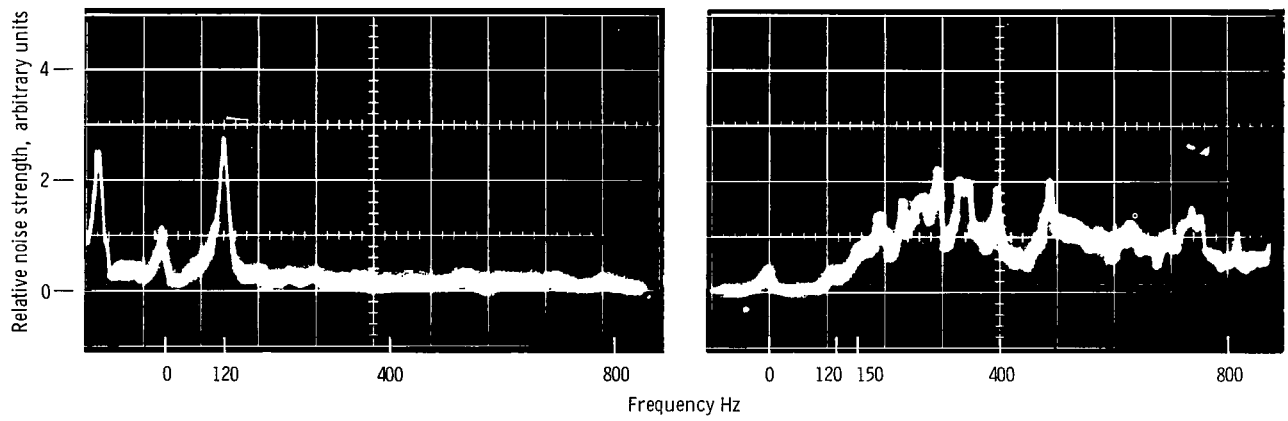

(a) Power supply peak (120 Hz). (b) Power supply noise (120 Hz), suppressed.

Figure 9. - Frequency spectrum analysis of power-supply noise for operating thruster.

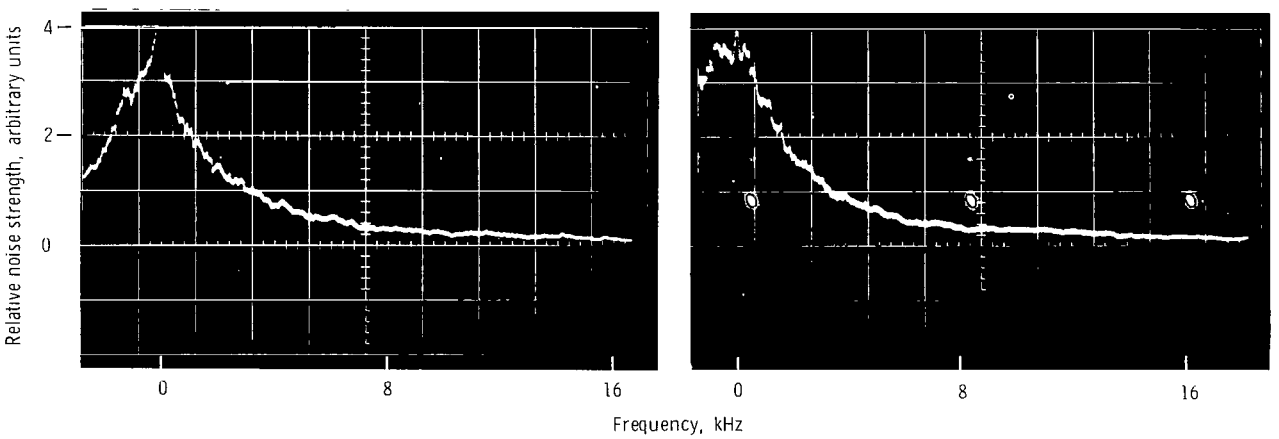

(a) Magnetic field, 1.8 milliteslas. (b) Magnetic field, 3.3 milliteslas.

Figure 10. - Frequency spectrum analysis of uniform magnetic field thruster for different magnetic field strength.

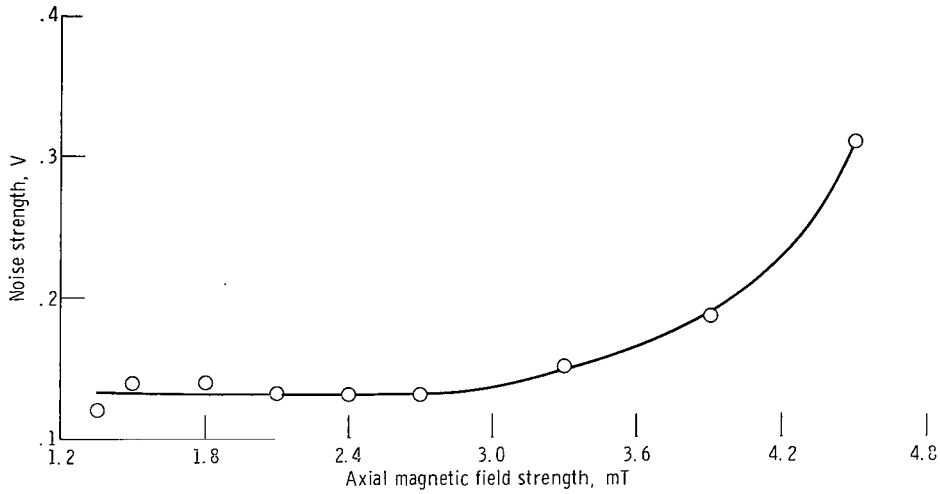

Figure 11. - Plasma noise strength as function of magnetic-field strength for uniform-field configuration. Noise was measured with an rms voltmeter.

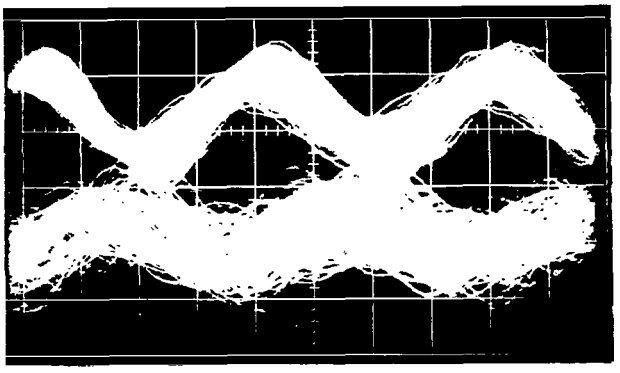

(a) Magnetic field, 3.9 milliteslas (R); frequency, 4.7 kilohertz; phase shift of lower trace, 125° leading.

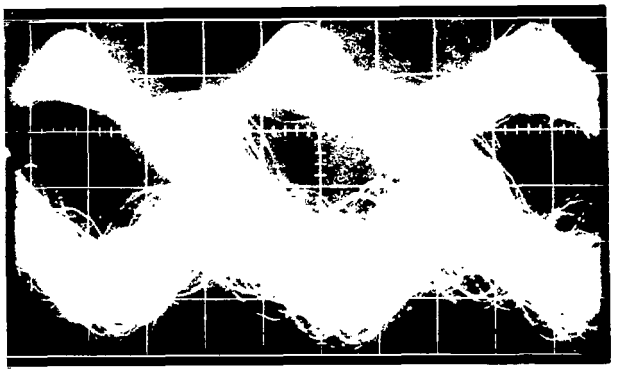

(b) Magnetic field, 3.9 milliteslas (N); frequency, 4.7 kilohertz; phase shift of lower trace, 125° lagging.

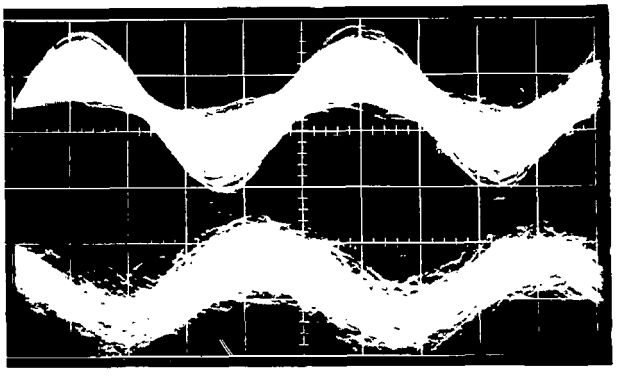

(c) Magnetic field, 3.9 milliteslas (N); frequency, 6.0 kilohertz; phase shift of lower trace, 150° lagging.

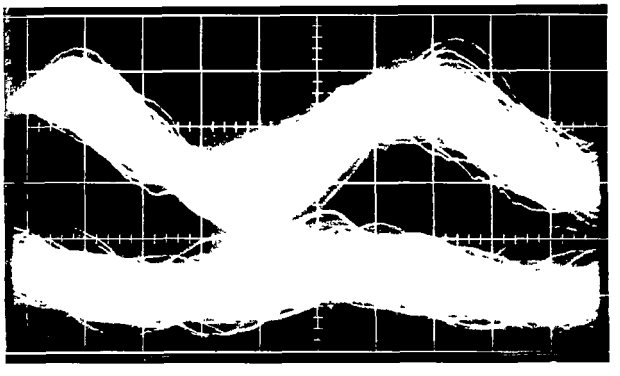

(d) Magnetic field, 3.9 milliteslas (N); frequency, 3 kilohertz; phase shift of lower trace, 84° lagging.

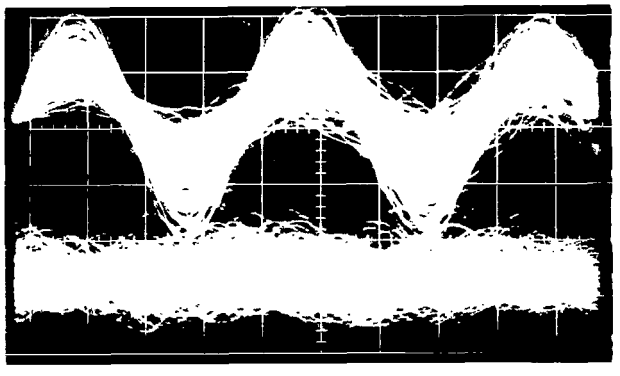

(e) Magnetic field, 3.9 milliteslas (R); frequency, 4.7 kilohertz; no correlation.

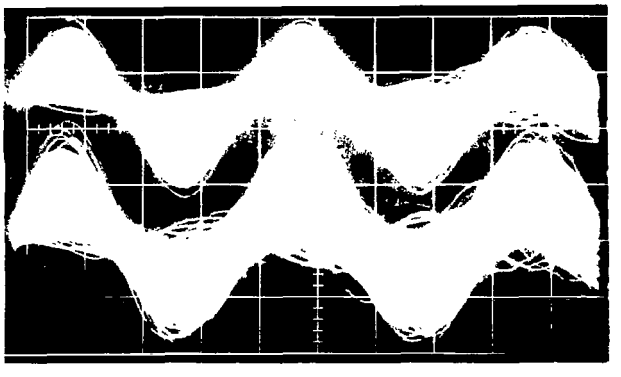

(f) Magnetic field, 3.9 milliteslas (N); frequency, 4.7 kilohertz; probes B and D; phase shift, zero.

Figure 12. - Correlation study for uniform-field thruster. Frequency values refer to signal component under analysis. N denotes normal magnetic field and R denotes reversed magnetic field. Probes A and B of figure 5 except where noted. Vertical settings, 1 to 200 millivolts per centimeter; horizontal settings, 50 microseconds per centimeter.

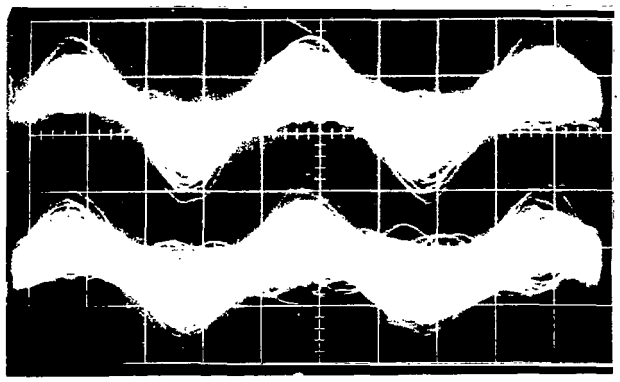

(g) Magnetic field, 3.9 milliteslas (R); frequency, 4.7 kilohertz; probes B and D; phase shift, zero.

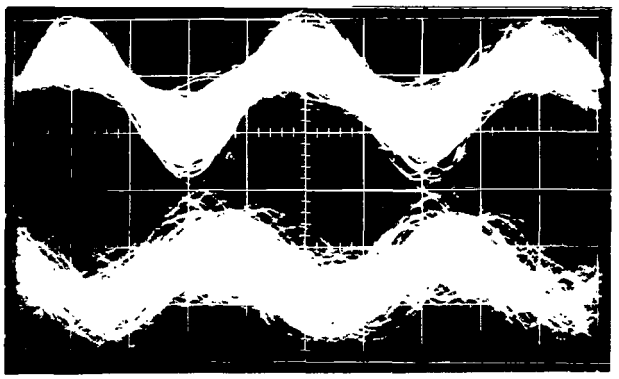

(h) Magnetic field, 2.1 milliteslas (N); frequency, 4.7 kilohertz; phase shift of lower trace, 145° lagging.

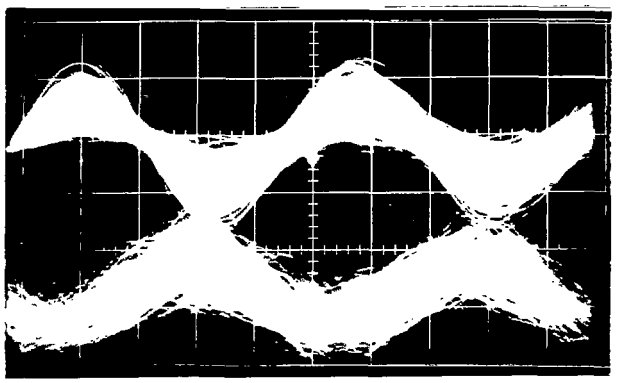

(i) Magnetic field, 2.1 milliteslas (R); frequency, 4.7 kilohertz; phase shift of lower trace, 155° leading.

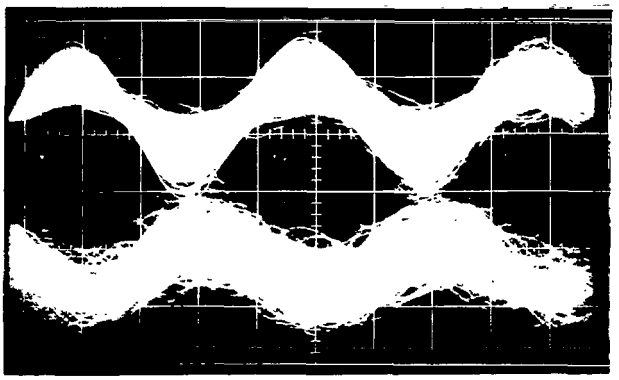

(j) Magnetic field, 1.8 milliteslas (R); frequency, 4.7 kilohertz; phase shift of lower trace, 207° leading.

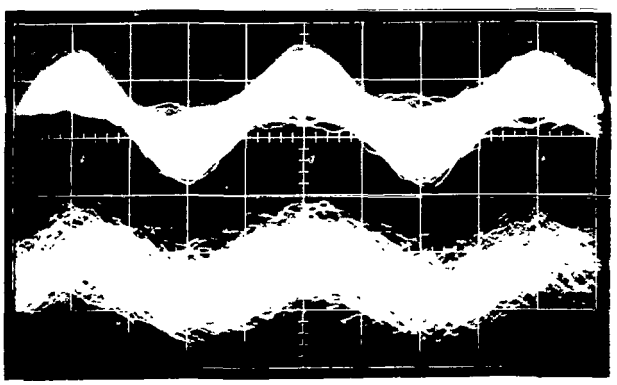

(k) Magnetic field, 1.5 milliteslas (N); frequency, 4.7 kilohertz; phase shift, zero.

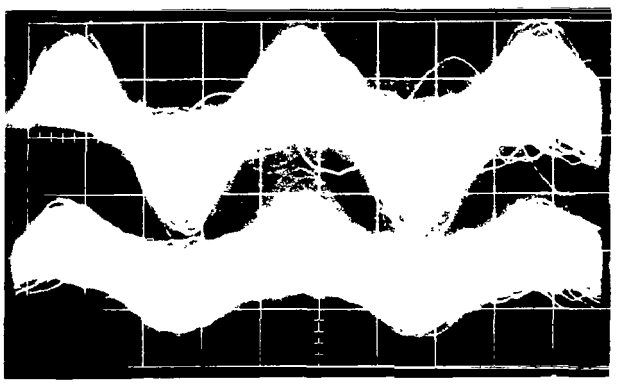

(l) Magnetic field, 1.8 milliteslas; frequency, 4.7 kilohertz; probes B and D; phase shift, zero.

Figure 12. - Concluded.

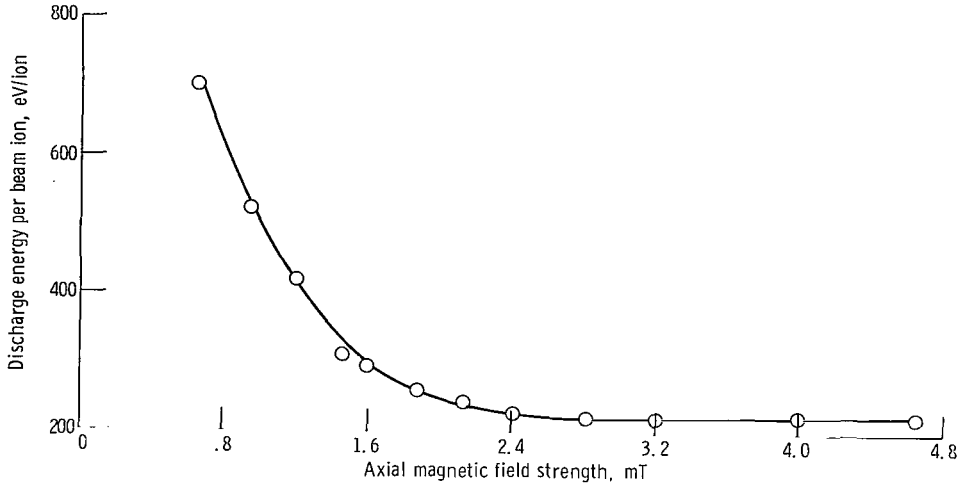

Figure 13. - Discharge energy per beam ion as function of magnetic field strength for nonuniform-field configuration and main anode operation, beam current, 200 milliamperes, neutral flow, 220 milliamperes.

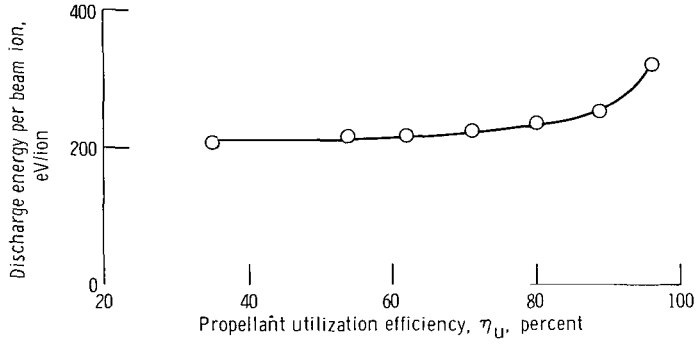

Figure 14. - Discharge energy per beam ion as function of propellant utilization efficiency for nonuniform-field configuration and main anode operation. Neutral flow, 280 milliamperes.

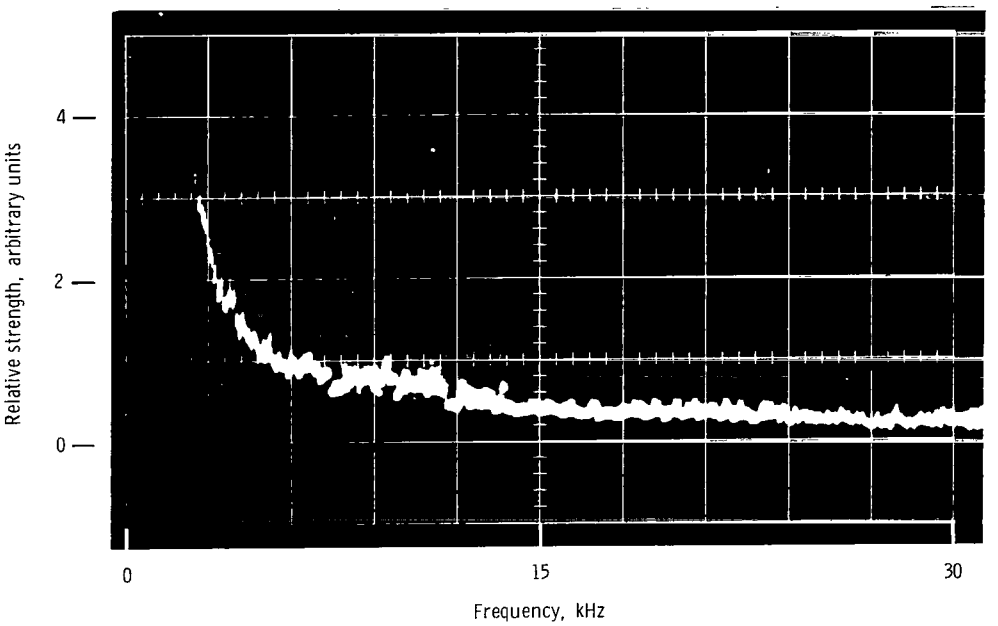

Figure 15. - Typical frequency spectrum for nonuniform-field operation and main anode operation. Magnetic field, 3.0 milliteslas.

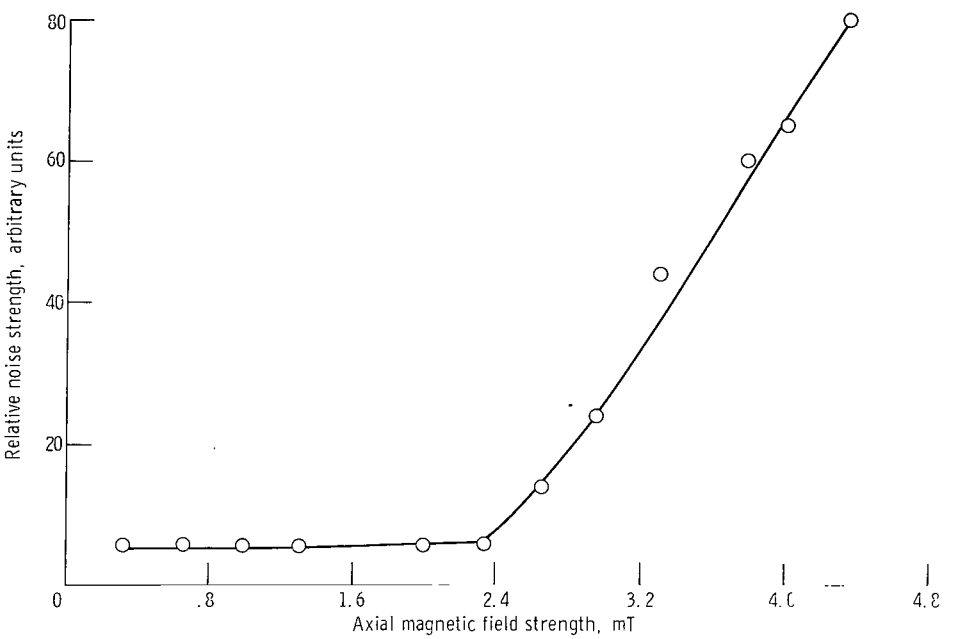

Figure 16. - Relative noise strength as function of magnetic-field strength for nonuniform-field configuration and main anode operation.

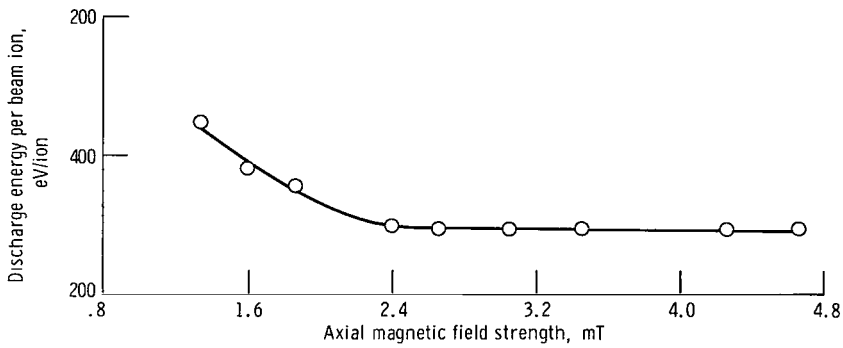

Figure 17. - Discharge energy per beam ion as function of magnetic field strength for the rear anode configuration. Beam current, 200 milliamperes; neutral flow, 555 milliamperes.

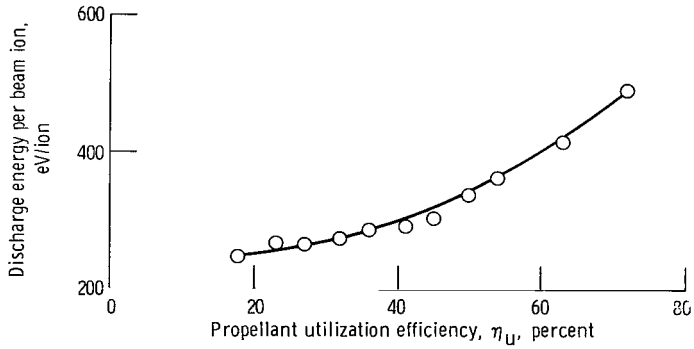

Figure 18. - Discharge energy per beam ion as function of propellant utilization efficiency for the rear anode configuration. Neutral flow, 555 milliamperes.

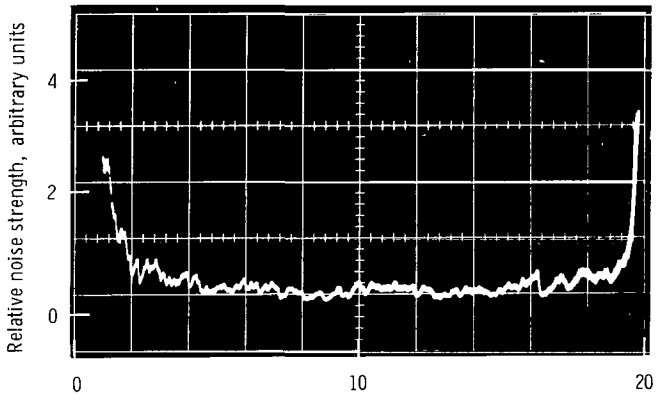

(a) Magnetic field, 1.8 milliteslas.

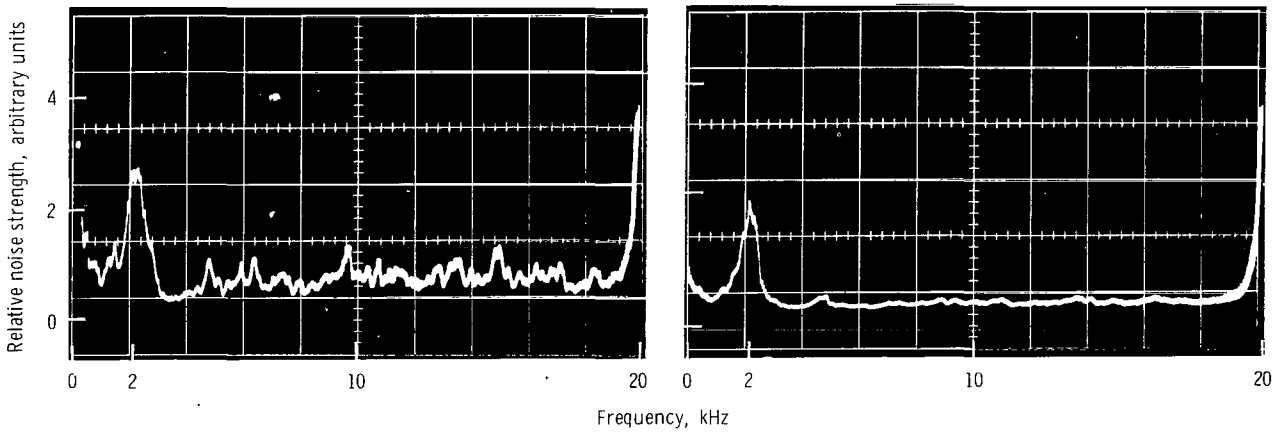

(b) Magnetic field, 2.4 milliteslas.

(c) Magnetic field, 2.7 milliteslas.

Figure 19. - Frequency spectrum analysis for nonuniform field configuration operating on the rear anode.

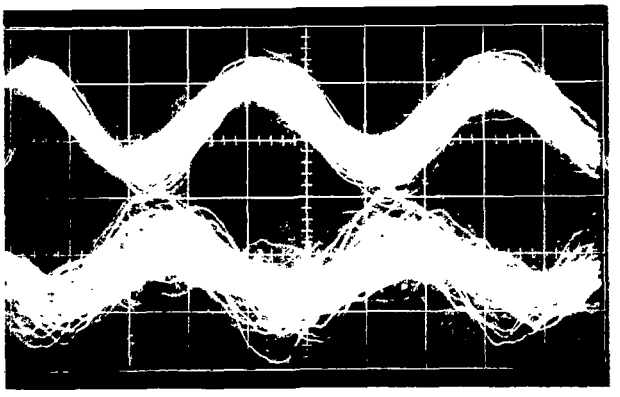

(a) Magnetic field strength, 2.8 milliteslas (N); probes A and B; component frequency 4.7 kilohertz; upper trace phase shift 117° lagging.

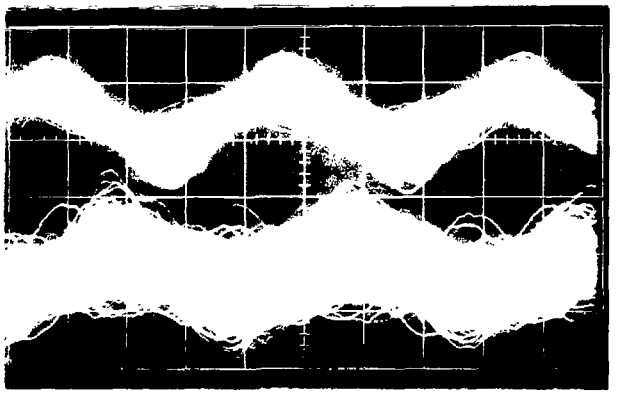

(b) Magnetic field strength, 2.8 milliteslas (R); probes A and B; component frequency 4.7 kilohertz; upper trace phase shift 123° leading.

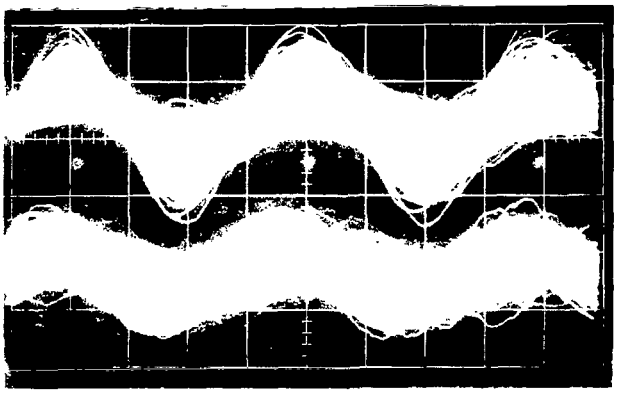

(c) Magnetic field strength, 2.8 milliteslas; probes B and D; component frequency 4.7 kilohertz; upper trace phase shift 45° lagging.

Figure 20. - Correlation study for nonuniform field configuration and main anode operation. Horizontal setting, 50 microseconds per centimeter; vertical setting, 100 milivolts per centimeter. N denotes normal magnetic field and R denotes reversed magnetic field.

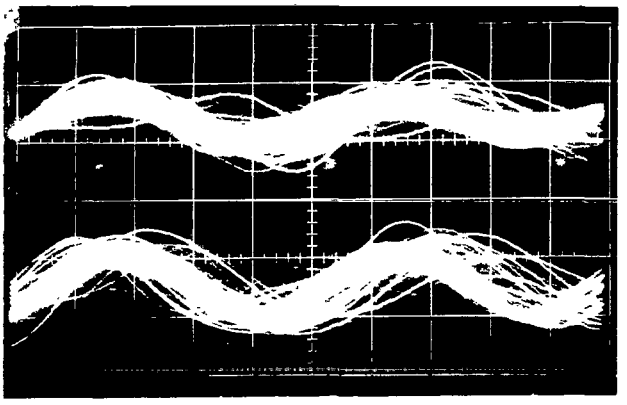

(a) Magnetic field, 2.9 milliteslas; probes C and D; component frequency, 2 kilohertz; phase shift, zero.

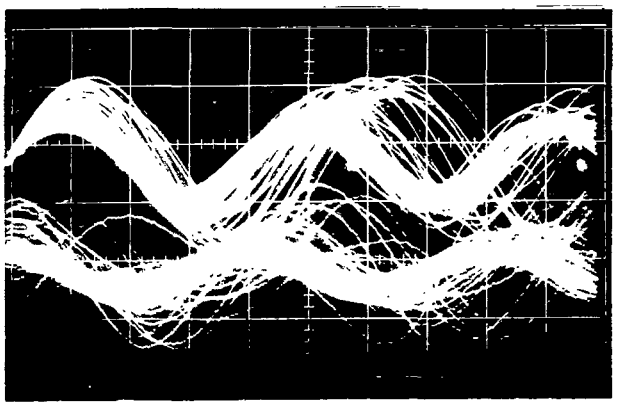

(b) Magnetic field, 2.9 milliteslas; probes C and transformer on main anode; component frequency, 2 kilohertz; phase shift, 90° lagging.

Figure 21. - Correlation study for nonuniform field configuration with rear anode operation. Horizontal setting, 0.1 millisecond per centimeter; vertical setting, 10 to 50 milivolts per centimeter.

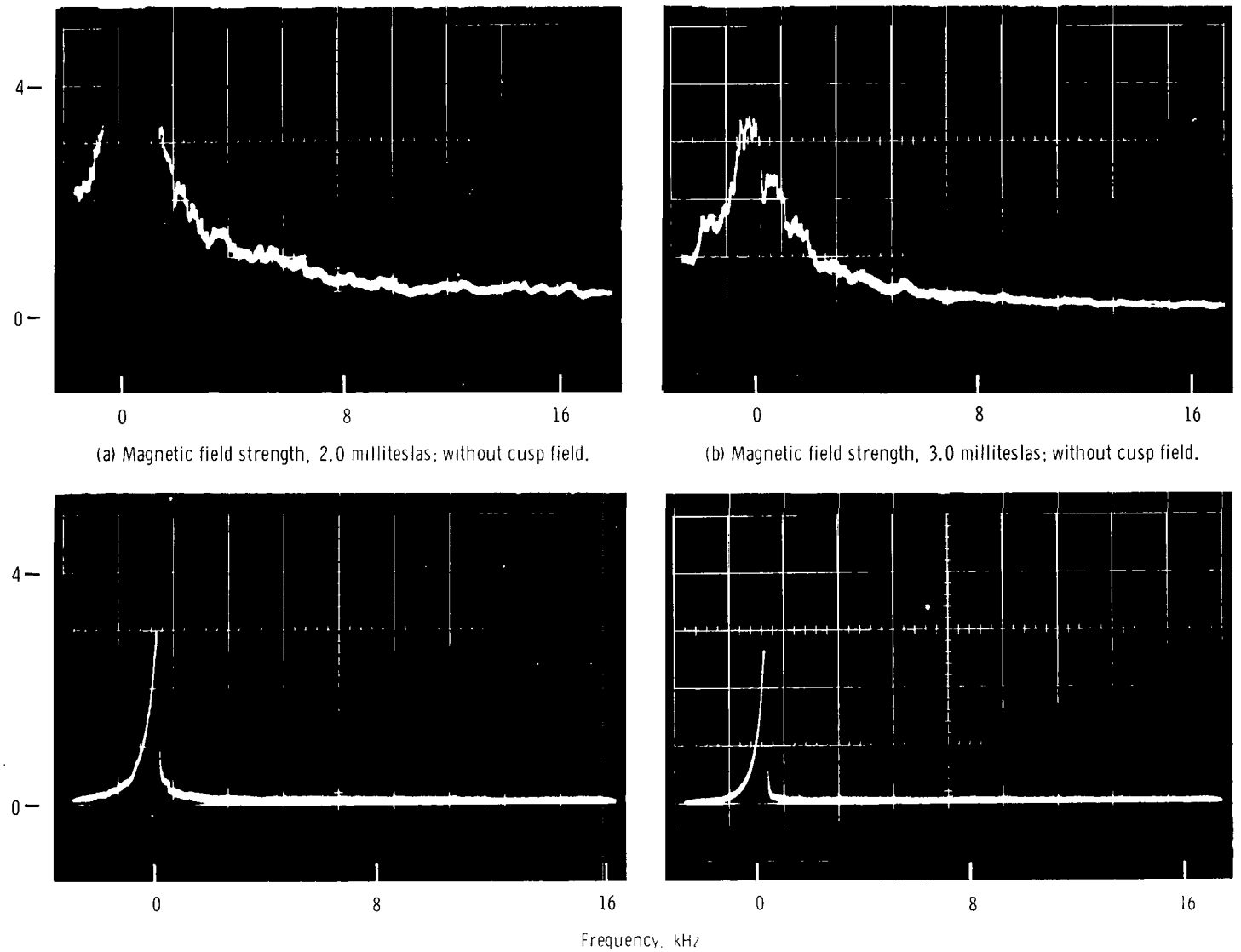

(a) Magnetic field strength, 2.0 milliteslas; without cusp field.

(b) Magnetic field strength, 3.0 milliteslas; without cusp field.

(c) Magnetic field strength, 2.0 milliteslas; cusp magnet current, 10 amperes.

(d) Magnetic field strength, 3.0 milliteslas; cusp magnet current, 10 amperes.

Figure 22. - Plasma noise strength study for nonuniform field operation with and without cusp field operating. Thruster configuration (3) (fig. 1(c)).

05U 001 50 51 3DS 71.10 00903
AIR FORCE WEAPONS LABORATORY /WLOL/
KIRTLAND AFB, NEW MEXICO 87117

ATT E. LOU BOWMAN, CHIEF,TECH. LIBRARY

"The aeronautical and space activities of the United States shall be conducted so as to contribute . . . to the expansion of human knowledge of phenomena in the atmosphere and space. The Administration shall provide for the widest practicable and appropriate dissemination of information concerning its activities and the results thereof."

—NATIONAL AERONAUTICS AND SPACE ACT OF 1958

NASA SCIENTIFIC AND TECHNICAL PUBLICATIONS

TECHNICAL REPORTS: Scientific and technical information considered important, complete, and a lasting contribution to existing knowledge.

TECHNICAL NOTES: Information less broad in scope but nevertheless of importance as a contribution to existing knowledge.

TECHNICAL MEMORANDUMS: Information receiving limited distribution because of preliminary data, security classification, or other reasons.

CONTRACTOR REPORTS: Scientific and technical information generated under a NASA contract or grant and considered an important contribution to existing knowledge.

TECHNICAL TRANSLATIONS: Information published in a foreign language considered to merit NASA distribution in English.

SPECIAL PUBLICATIONS: Information derived from or of value to NASA activities. Publications include conference proceedings, monographs, data compilations, handbooks, sourcebooks, and special bibliographies.

TECHNOLOGY UTILIZATION PUBLICATIONS: Information on technology used by NASA that may be of particular interest in commercial and other non-aerospace applications. Publications include Tech Briefs, Technology Utilization Reports and Technology Surveys.

Details on the availability of these publications may be obtained from:

SCIENTIFIC AND TECHNICAL INFORMATION OFFICE

NATIONAL AERONAUTICS AND SPACE ADMINISTRATION

Washington, D.C. 20546